

## Magnetic interaction in Co-doped SnO<sub>2</sub> nano-crystal powders

This article has been downloaded from IOPscience. Please scroll down to see the full text article.

2006 J. Phys.: Condens. Matter 18 6001

(<http://iopscience.iop.org/0953-8984/18/26/018>)

View [the table of contents for this issue](#), or go to the [journal homepage](#) for more

Download details:

IP Address: 129.252.86.83

The article was downloaded on 28/05/2010 at 11:59

Please note that [terms and conditions apply](#).

# Magnetic interaction in Co-doped SnO<sub>2</sub> nano-crystal powders

C M Liu<sup>1,4</sup>, X T Zu<sup>1,2</sup> and W L Zhou<sup>3</sup>

<sup>1</sup> Department of Applied Physics, University of Electronic Science and Technology of China, Chengdu 610054, People's Republic of China

<sup>2</sup> International Center for Material Physics, Chinese Academy of Sciences, Shenyang 110015, People's Republic of China

<sup>3</sup> Advanced Materials Research Institute, University of New Orleans, New Orleans, Louisiana 70148, USA

E-mail: [cmliu@uestc.edu.cn](mailto:cmliu@uestc.edu.cn)

Received 18 March 2006, in final form 15 May 2006

Published 19 June 2006

Online at [stacks.iop.org/JPhysCM/18/6001](http://stacks.iop.org/JPhysCM/18/6001)

## Abstract

Rutile-type Co-doped SnO<sub>2</sub> nano-crystal powders are prepared by the wet chemical method. The magnetic moment is found to decrease with increasing Co content. There is hysteresis between field cooled (FC) and zero field cooled (ZFC) magnetization when the temperature is below 70 K. These magnetic behaviours represent antiferromagnetic interaction between Co ions. By measuring the magnetization as a function of temperature, the magnetic interaction between Co ions is evaluated qualitatively using the Curie–Weiss law. The value of the effective exchange integral  $J_1/k_B$  is about  $-62$  K, indicating a very strong antiferromagnetic superexchange interaction between Co ions.

## 1. Introduction

Functional spintronic devices, such as spin light-emitting diodes, have been demonstrated using II–VI and III–V diluted magnetic semiconductors (DMSs) as the pivotal spin-injection components, but to date these devices have been operable only at cryogenic temperatures because of either the absence of ferromagnetism or the low Curie temperature ( $T_c$ ) for the ferromagnetic phase transition [1, 2]. Thus, there is an ongoing quest for ferromagnetic semiconductors with a  $T_c$  well above room temperature. Much recent interest has been generated by high-temperature ferromagnetism in oxide and nitride materials [3–5], promising potential applications in the field of spintronics and optospintronics. Although there have been very few reports on SnO<sub>2</sub>-based DMSs compared to other oxide-based DMSs [5], many interesting properties have been observed, such as a giant magnetic moment [6] and

<sup>4</sup> Author to whom any correspondence should be addressed; Tel: 86-028-83202130.

large coercivity [7]. Moreover, the origin of magnetism still remains a question [8]. The magnetization of  $\text{Sn}_{1-x}\text{Mn}_x\text{O}_2$  (moments per Mn site) is found to decrease with increasing  $x$ , representing the antiferromagnetic nature of the Mn–O–Mn interaction reminiscent of the antiferromagnetism in rutile  $\text{MnO}_2$  [9]. On the other hand, the magnetic moment is also seen to drop rapidly with increasing Co content, and is attributed to the enhanced dopant–dopant associations leading to progressive orbital moment quenching [6].

To our knowledge, there have been no reports on the quantitative evaluation of the intrinsic exchange coupling between magnetic ions for transition metal-doped  $\text{SnO}_2$  powders. In this paper we present a systematic study of the structure and the magnetic interaction of Co-doped  $\text{SnO}_2$  nano-crystal powders. It is found that the value of the effective exchange integral  $J_1/k_B$  is about  $-62$  K, indicating a very strong antiferromagnetic superexchange interaction between Co ions.

## 2. Experiments

Co-doped  $\text{SnO}_2$  nano-powders were successfully prepared by means of dissolving tin chloride (hydrous  $\text{SnCl}_4 \cdot 5\text{H}_2\text{O}$  analytic reagent (AR)) and cobalt chloride (hydrous  $\text{CoCl}_2 \cdot 6\text{H}_2\text{O}$  analytic reagent (AR)) in distilled water. In a typical synthesis, an aqueous ammonia solution was added to the above solution dropwise. The dropping rate must be well controlled for the chemical homogeneity. The resulting gel was collected, washed with distilled water, and then dried at  $100^\circ\text{C}$  for several hours. Heating treatments of the synthesized nano-powders were conducted at  $350^\circ\text{C}$  for 1 h.

The crystalline structure of the material was analysed by x-ray diffraction (XRD) using a Rigaku D/max-2400 diffractometer with a curved crystal monochromator and  $\text{Cu K}\alpha$  radiation ( $=0.154056$  nm) operated at 40 kV and 60 mA. The feature micrographs were obtained using an H-600 transmission electron microscopy (TEM) operated at 100 kV. The samples' stoichiometry was measured by a KRATOS X SAM 800 x-ray photoelectron spectroscopy (XPS) system. After the as-produced powders were well dispersed in distilled water suspension by using a supersonic disperser, the absorption spectra of the samples were measured on a Shimadzu UV-2500 ultraviolet–visible spectrophotometer. The magnetism is measured using a Lakeshore 7400 vibrating sample magnetometer (VSM) and superconducting quantum interference device (SQUID).

## 3. Results and discussion

XRD patterns of  $\text{Sn}_{1-x}\text{Co}_x\text{O}_2$  (with  $x = 0.005, 0.02$  and  $0.10$ ) are shown in figure 1. As seen in figure 1, x-ray diffraction measurements reveal that the structures of all the samples are a rutile-type cassiterite (tetragonal) phase of  $\text{SnO}_2$ , and the doping does not change the tetragonal structure of  $\text{SnO}_2$ . Furthermore, we could not find any trace of an impurity phase in the XRD measurement. The peak positions do not show any measurable change, while the intensities of the peaks decrease with increasing Co content. As Co content increases, the XRD peaks appear to be wider, indicating possible changes in the crystallite size and/or strain. This is similar to that reported in [7]. Using the Scherrer equation, the crystal size can be estimated. The crystal sizes determined from the (110) diffraction peak are 6, 4.9 and 4.5 nm for  $x = 0.005, 0.02$  and  $0.10$ , respectively.

Figure 2 illustrates the TEM microscopy and the corresponding electron diffraction (ED) pattern of  $\text{Sn}_{0.995}\text{Co}_{0.005}\text{O}_2$ . Except that of pure  $\text{SnO}_2$ , there is no other impurity phase present, as indicated by the ED pattern. The TEM image reveals significant aggregation of the nano-particles. The aggregation is critical for the ferromagnetism in nano-crystalline oxides [10], which can increase the domain volumes and generate lattice defects. The

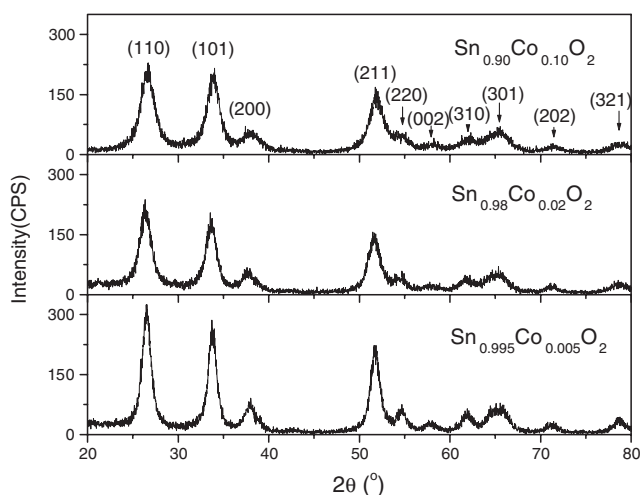


**Figure 1.** XRD patterns of  $\text{Sn}_{1-x}\text{Co}_x\text{O}_2$  (with  $x = 0.005, 0.02$  and  $0.10$ ). There is no trace of an impurity phase, except that of rutile-type  $\text{SnO}_2$ . Diffraction peaks get wider and their intensity decreases with increasing Co content.

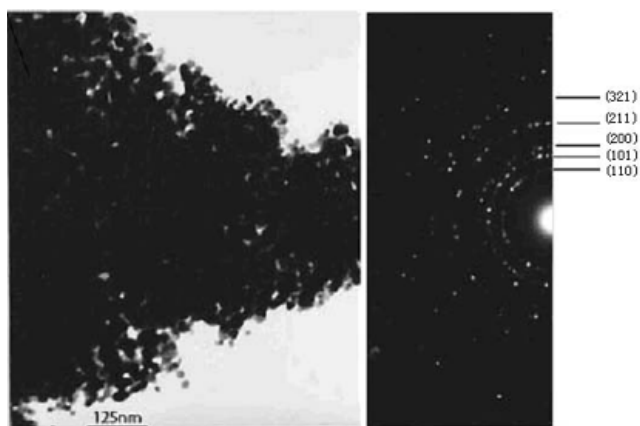


**Figure 2.** TEM microscopy and the corresponding electron diffraction (ED) pattern of  $\text{Sn}_{0.995}\text{Co}_{0.005}\text{O}_2$ .

significant aggregation in our samples should be promising for magnetism. The aggregation makes it difficult to determinate the particle size accurately. The size that is estimated from the individual spherical particle is about 10 nm. This is slightly larger than that obtained from XRD measurements.

The hysteresis of samples with various dopant concentration ( $x$ ) is measured by VSM. The maximum magnetic field applied in the measurements is about 10 000 Oe. The sample's mass ( $m$ ) is measured using a balance. The average magnetic moment per mol ( $\sigma$ ) at the maximum applied field is obtained using  $\sigma = \frac{M_H}{m} \times [118.69 \times (1 - x) + 58.93x + 32]$ , in which  $M_H$  is the magnetic moment at the maximum applied field. The magnetic moment per Co ion is calculated using equation (1), in which  $N_A$  represents the molecular number of 1 mol sample. As illustrated by figure 3, the magnetic moment per Co ion decreases with increasing  $x$ , which

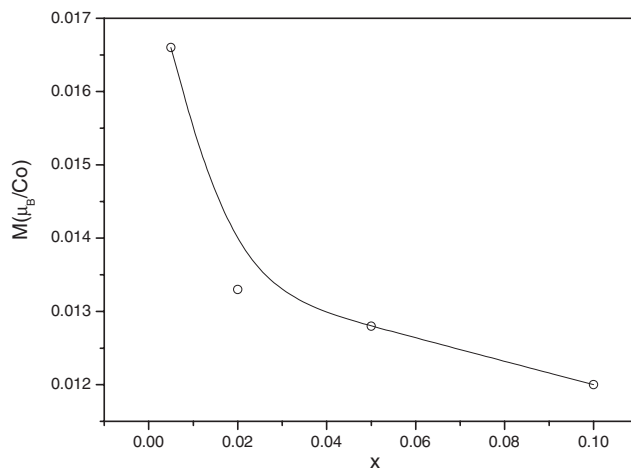


**Figure 3.** Magnetic moment per Co ion as a function of Co content  $x$ . The solid line is a guide for the eye.

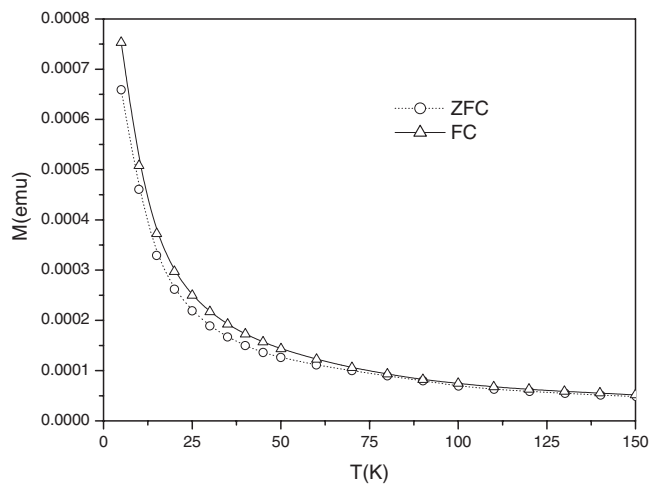


**Figure 4.** ZFC and FC magnetization as a function of temperature for  $\text{Sn}_{0.995}\text{Co}_{0.005}\text{O}_2$ . The magnetization is measured at a constant field of 500 Oe.

might represent an antiferromagnetic interaction between Co ions like that in [9]:

$$M = \frac{\sigma}{N_A x}. \quad (1)$$

Figure 4 shows the zero field cooled (ZFC) and field cooled (FC) magnetization as a function of temperature for  $\text{Sn}_{0.995}\text{Co}_{0.005}\text{O}_2$ . The magnetization is measured at a constant field of 500 Oe. As seen from figure 4, there is hysteresis between FC and ZFC magnetization when the temperature is below 70 K. According to reference [11, 12], the bifurcation of the FC and ZFC data below 70 K might be a manifestation of the antiferromagnetic interaction.

For a quantitative evaluation of the intrinsic exchange coupling between Co ions, Curie-Weiss plots are made from the inverse magnetization data obtained from the FC  $M$ - $T$  curves in a magnetic field of 500 Oe for  $\text{Sn}_{0.995}\text{Co}_{0.005}\text{O}_2$ , as shown in figure 5. According to the

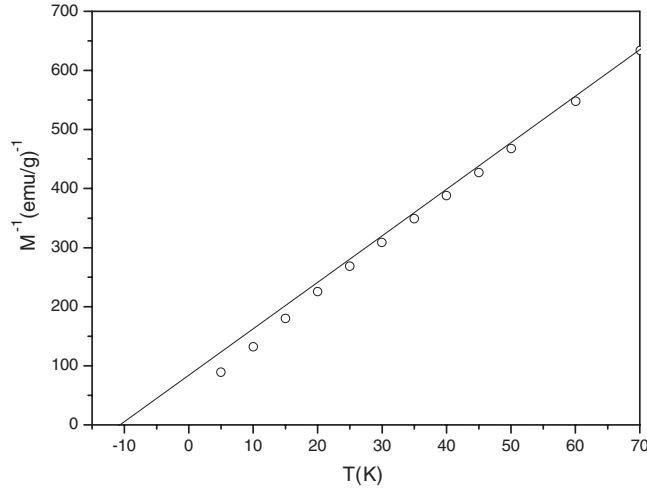


**Figure 5.** The inverse magnetization data obtained from the FC  $M$ - $T$  curve. The solid line is a linear fit for the higher-temperature region.

discussion of [13, 14], the Curie–Weiss law can be expressed as

$$\frac{1}{M} = \frac{T - \Theta(x)}{C(x)H} \quad (2)$$

with the Curie constant  $C(x)$  given by

$$C(x) = xC_0 = x(g\mu_B)S(S+1)n/3k_B \quad (3)$$

and the Curie–Weiss temperature  $\Theta(x)$  expressed as

$$\Theta(x) = x\Theta_0 = 2xS(S+1)zJ_1/3k_B \quad (4)$$

where  $x$  is the content of the Co<sup>2+</sup> ions,  $n$  is the number of cation sites per unit volume,  $z$  is the number of the nearest-neighbour cations ( $z = 14$  for the rutile structure),  $k_B$  is the Boltzmann constant,  $\mu_B$  is the Bohr magneton,  $S$  is the value of spin for the Co<sup>2+</sup> ions in SnO<sub>2</sub>, and  $J_1$  is the effective exchange integral between nearest-neighbour Co<sup>2+</sup> ions.

The Curie–Weiss temperature,  $\Theta(x)$ , can be obtained by extending the linear part in figure 5 to zero inverse magnetization, which is evaluated to be  $-10.9$  K. The value of  $\Theta_0$ , which is the Curie–Weiss temperature for  $x = 1$ , is estimated to be  $-2180$  K, and the value of  $J_1/k_B$  is then evaluated as  $-62$  K from equation (4) using the value of  $S = 3/2$  for the Co<sup>2+</sup> ions in the high spin state. The negative values of  $\Theta_0$  and  $J_1$ , indicating an antiferromagnetic interaction between Co ions, suggests that superexchange is the likely fundamental mechanism in Co-doped SnO<sub>2</sub> nano-crystal powders. Besides the superexchange interaction, there may be other types of interactions, such as the Ruderman–Kittel–Kasuya–Yosida (RKKY) interaction mediated by holes [15] or the ferromagnetic interaction mediated by F-centre exchange [8]. We note that the magnitude of  $J_1/k_B$  is almost the same as that of Zn<sub>1-x</sub>Co<sub>x</sub>Se ( $-54 \pm 8$  K) [16]. In addition, the magnitude of  $\Theta_0$  for Mn-doped ZnO is  $-1900$  K [17], which is close to our results. Spin-glass behaviour has been discovered in Co and Mn-doped ZnO [14, 17], in which antiferromagnetic superexchange coupling is fundamental. It is expected that there is spin-glass behaviour in our samples. We will study this later.

According to the study of Ga<sub>1-x</sub>Mn<sub>x</sub>As by Priour *et al* [18], the antiferromagnetic coupling ( $J^{\text{AFM}}$ ) between Mn ions plays an important role for the ferromagnetic transition

temperature ( $T_c$ ), which can suppress  $T_c$  substantially depending on the precise value of the  $J^{\text{AFM}}$ . Meanwhile, the temperature dependence of spontaneous magnetization ( $M(T)$ ) depends on the probability distribution of the coupling between Mn ions ( $P(J)$ ). The degree of concavity in  $M(T)$  is strongly correlated to the multi-modal profile of  $P(J)$  and the weight extent of  $P(J)$  near zero interaction strength. The multi-modal profile of  $P(J)$  in general leads to a concave  $M(T)$ . Besides this, concavity in  $M(T)$  is a signature for small free-carrier density ( $n_c$ ) and small mean free path ( $r_0$ ), while convex profiles appear deep in the large  $n_c$  and large  $r_0$ . For intermediate  $n_c$  and  $r_0$ , it is possible to obtain a linear  $M(T)$  curve. Similar to the influence of  $J^{\text{AFM}}$  on  $T_c$  and the  $M(T)$  of  $\text{Ga}_{1-x}\text{Mn}_x\text{As}$  [18], the present finding of antiferromagnetic coupling between Co ions should have the same effect on  $T_c$  and the concavity in  $M(T)$  of Co-doped  $\text{SnO}_{2-\delta}$  thin films in [6]. However, the precise role played by antiferromagnetic coupling on ferromagnetic transitions in [6] is currently not very clear. It is interesting to note that the doping of Co causing an increase in the resistivity of Co-doped  $\text{SnO}_{2-\delta}$  films [6]. This will result in a change in  $n_c$ ,  $r_0$ ,  $T_c$  and a convex  $M(T)$ . On the other hand, the antiferromagnetic coupling between nearest-neighbour magnetic ions might be another reason for the decrease in the magnetic moment caused by an increase in dopant concentration [6]. With increasing dopant concentration, the number of magnetic ions occupying adjacent cation lattice positions increases. Therefore, the antiferromagnetic coupling results in the magnetic moments being antiferromagnetically aligned, leading to a reduction in the average magnetic moment per magnetic ion [19]. As stated previously, there may be other types of interaction between Co ions in  $\text{Sn}_{1-x}\text{Co}_x\text{O}_2$ , such as the RKKY interaction and F-centre exchange. Since our samples are in nano-crystal powder form, the mean free path and free-carrier density might be smaller than those in Co-doped  $\text{SnO}_{2-\delta}$  films [6]. This should cause carrier-mediated interaction in our samples to be smaller than that in Co-doped  $\text{SnO}_{2-\delta}$  films [6]. Furthermore, the dominating interaction mechanism might be different for nano-powder form samples and thin films. The dopant concentration dependence of the interaction is also dependent on the sample's form and fabrication methods.

The principal idea of superexchange is based on the notion of the admixture of the p-wave function representing the completely filled anion band to the neighbouring 3d states of magnetic ions. Spalek *et al* [13] argued that superexchange coupling is the fundamental mechanism determining the magnetic behaviour of II–VI DMSs. Recently, superexchange coupling has been considered to explain the magnetic behaviour of Co-doped ZnO DMSs [14]. The mechanism of superexchange coupling in our samples might be similar to that proposed by Spalek, however more work needs to be done to clarify it. In addition, the role played by Sn ions is currently unclear.

#### 4. Conclusion

In this work, it is found that Co-doped  $\text{SnO}_2$  powders have the rutile-type structure of pure  $\text{SnO}_2$ . The magnetic moment per Co ion decreases with increasing Co content. The exchange coupling between Co ions is evaluated qualitatively and found to be strongly antiferromagnetic, indicating that superexchange coupling is the most likely fundamental mechanism for our samples.

#### Acknowledgments

This study was supported financially by the NSAF Joint Foundation of China (10376006) and by the Program for New Century Excellent Talents in University and by the PhD funding support program of Education Ministry of China (20050614013).

## References

- [1] Stroud R M, Hanbicki A T, Park Y D, Kioseoglou G, Petukhov A G, Jonker B T, Itskos G and Petrou A 2002 *Phys. Rev. Lett.* **89** 166602
- [2] Jonker B T, Park Y D, Bennett B R, Cheong H D, Kioseoglou G and Petrou A 2000 *Phys. Rev. B* **62** 8180
- [3] Dietl T, Ohno H, Matsukura F, Cibert J and Ferrand D 2000 *Science* **287** 1019
- [4] Wolf S A, Awschalom D D, Buhanan R A, Daughton J M, Von Molnar S, Roukes M L, Chtchelkanova A Y and Treger D M 2001 *Science* **294** 1488
- [5] Fukumura T, Yamada Y, Toyosaki H, Hasegawa T, Hoinuma H and Kawasaki M 2004 *Appl. Surf. Sci.* **223** 62
- [6] Ogale S B, Choudhary R J, Buban J P, Lofland S E, Shinde S R, Kale S N, Kulkarni V N, Higgins J, Lanci C, Simpson J R, Browning N D, Das Sarma S, Drew H D, Greene R L and Venkatesan T 2003 *Phys. Rev. Lett.* **91** 077205
- [7] Punnoose A, Hays J, Gopal V and Shutthanandan V 2004 *Appl. Phys. Lett.* **85** 1559
- [8] Coey J M D, Douvalis A P, Fitzgerald C B and Venkatesan M 2004 *Appl. Phys. Lett.* **84** 1332
- [9] Kimura H, Fukumura T, Kawasaki M, Inaba K, Hasegawa T and Koinuma H 2002 *Appl. Phys. Lett.* **80** 94
- [10] Radovanovic P V and Gamelin D R 2003 *Phys. Rev. Lett.* **91** 157202
- [11] Manivannan A, Seehra M S, Majumder S B and Katiyar R S 2003 *Appl. Phys. Lett.* **83** 111
- [12] Punnoose A, Hays J, Gopal V and Shutthanandan V 2004 *Appl. Phys. Lett.* **85** 1559
- [13] Lewicki S A, Tarnawski Z, Furdyna J K, Galazka R R and Obuszko Z 1986 *Phys. Rev. B* **33** 3407–18
- [14] Kim J H, Kim H, Kim D, Yoon S G and Choo W K 2004 *Solid State Commun.* **131** 677
- [15] Matsukura F, Ohno H, Shen A and Sugawara Y 1998 *Phys. Rev. B* **57** R2037
- [16] Lewicki A and Schindler A I 1989 *Phys. Rev. B* **40** 2379–82
- [17] Fukumura T, Jin Z, Kawasaki M, Shono T, Hasegawa T, Koshihara S and Koinuma H 2001 *Appl. Phys. Lett.* **78** 958
- [18] Priour D J Jr, Hwang E H and Das Sarma S 2004 *Phys. Rev. Lett.* **92** 117201
- [19] Buchholz D B and Chang R P H 2005 *Appl. Phys. Lett.* **87** 082504